Electronic Supplementary Material (ESI) for Journal of Materials Chemistry A.

Supplementary Material

Architectural design and phase engineering of N/B-codoped TiO_2(B)/anatase nanotube assemblies for high-rate and long-life lithium storage

Chaoji Chen,[a] **Xianluo Hu**,[a,*] **Bao Zhang**,[b] **Ling Miao**[b] **and Yunhui Huang**[a,*]

[a] State Key Laboratory of Materials Processing and Die & Mould Technology, School of Materials Science and Engineering, Huazhong University of Science and Technology, Wuhan 430074, P. R. China

[b] Wuhan National Laboratory for Optoelectronics, and School of Optical and Electronic Information, Huazhong University of Science and Technology, Wuhan 430074, P. R. China

*Correspondence to: huxl@mail.hust.edu.cn

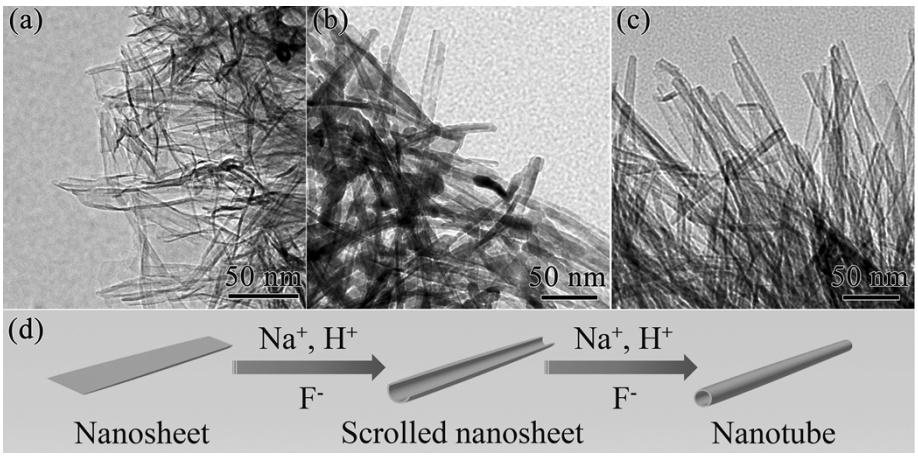

Fig. S1. TEM images of the products prepared for different ionothermal reaction time: (a) 6 h, (b) 12 h, and (c) 30 h. (d) Illustration of the time-dependent morphology evolution.

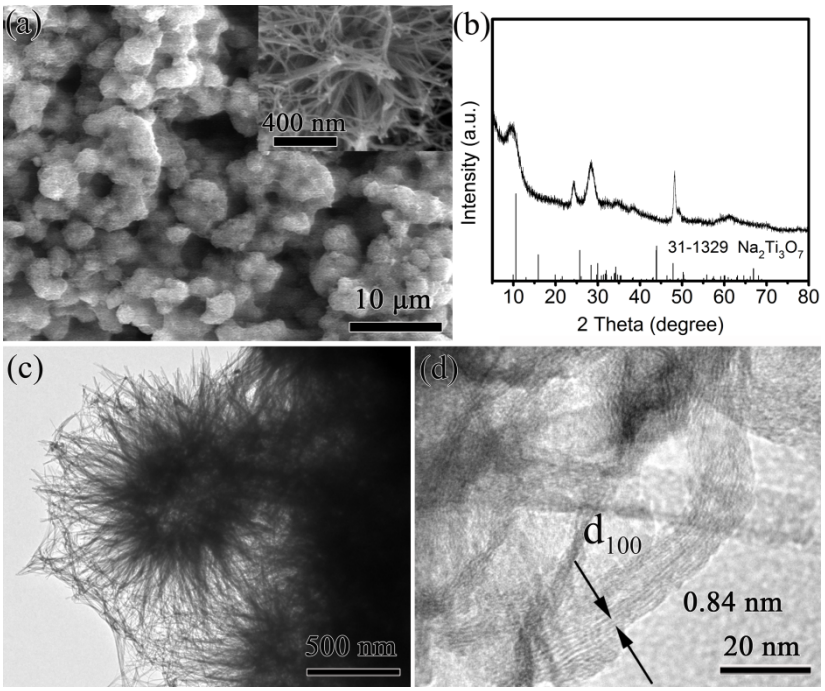

Fig. S2. (a) SEM image (inset shows the magnified SEM image), (b) XRD pattern, (c) TEM image, and (d) HRTEM image for the $Na_2Ti_3O_7$ (NTO) product.

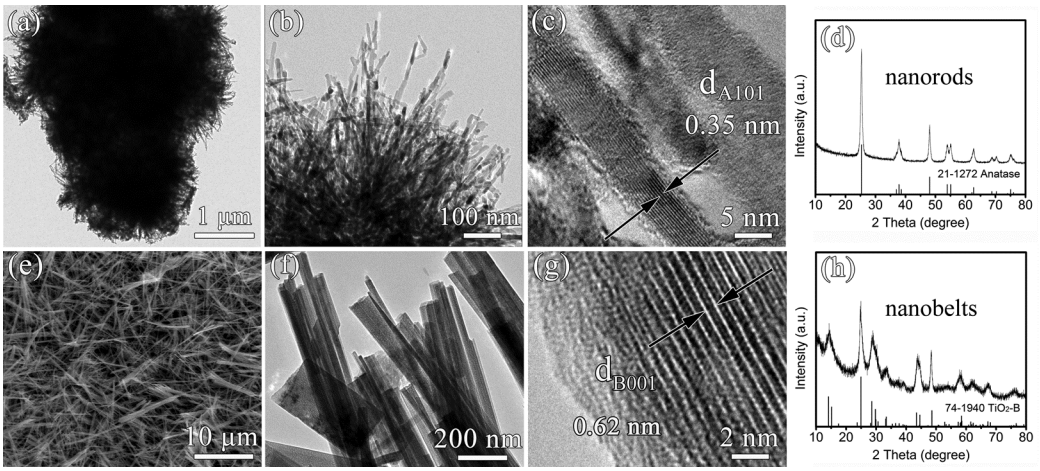

Fig. S3. (a,b,c,d) SEM, TEM, HRTEM images and XRD pattern for the TiO_2 nanorod assemblies. (e,f,g,h) TEM, HRTEM images and XRD pattern for the TiO_2(B) nanobelts.

Fig. S4. Volume comparison of the TiO_2 nanotube assemblies and the TiO_2(B) nanobelts with the same mass.

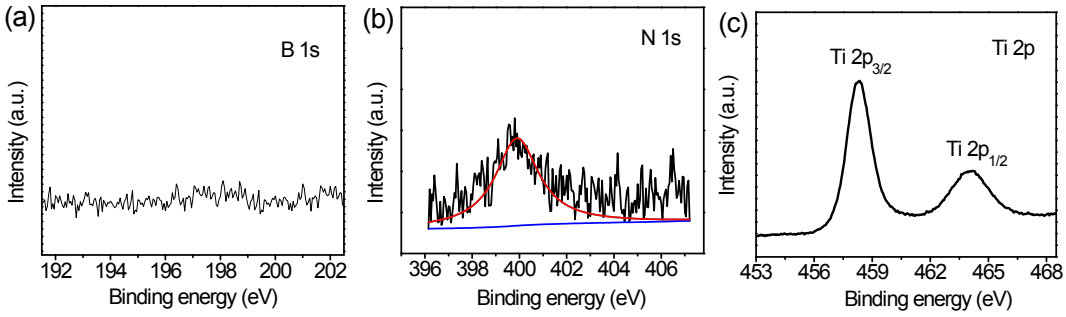

Fig. S5. High resolution XPS spectra of TiO_2 nanorod assemblies: (a) B 1s; (b) N 1s; and (c) Ti 2p.

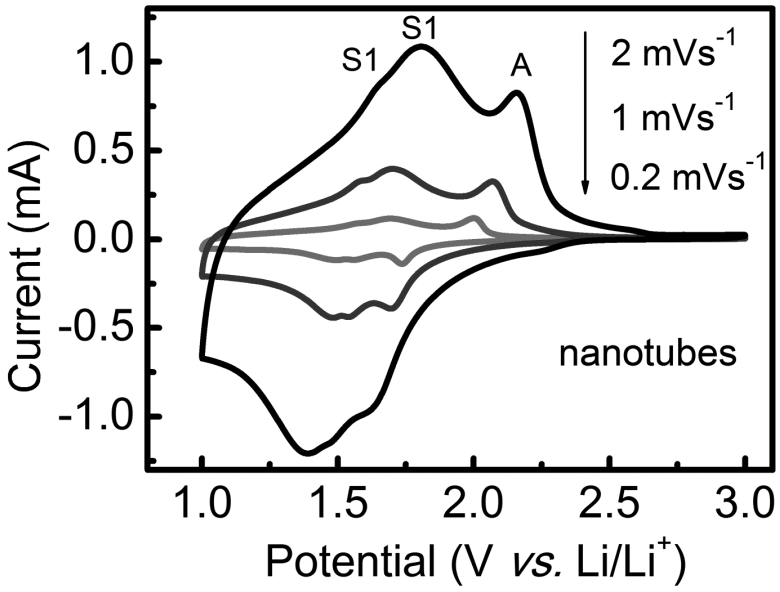

Fig. S6. CV curves of the TiO_2 nanotube assemblies at different scan rates.

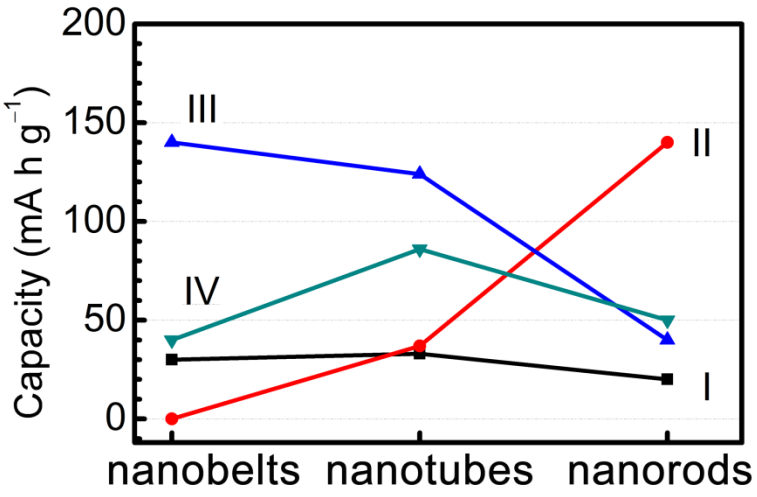

Fig. S7. Capacity contribution varies upon the TiO_2 products from Region I to IV.

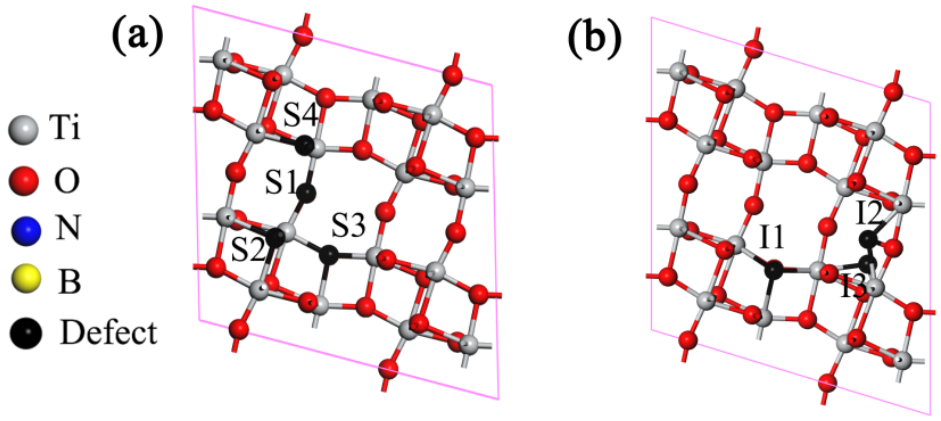

Fig. S8. Possible N/B doping sites in TiO_2(B). (a) O atoms substituted sites by nitrogen or boron; (b) interstitial sites for nitrogen doping.

Supplementary Method: DFT calculation details

Considering the majority of the phase composition in the product of TiO_2 nanotube assemblies is TiO_2(B) (~81%), only TiO_2(B) was taken into account in the first principle calculations. Nitrogen (~2 at.%) can be located in the lattice of TiO_2 interstitially or substitutionally and boron (~1 at.%) can be located in substitutionally combining our XPS results. The formation possibilities of three types of doping are investigated.

To discuss the N-doped TiO_2, we calculated interstitial and substitutional sites respectively. The possible substitutional and interstitial doping sites are shown in Figure S8a and b, respectively. The following formulas are used to calculate the N-doped formation energy, E_f, and listed in Table S1.

For O atoms substituted by nitrogen:

$$E_f = E_{doped-TiO_2} - E_{bulk-TiO_2} - \frac{1}{2}E_{N_2(g)} + \frac{1}{2}E_{O_2(g)}$$

For interstitial nitrogen doping:

$$E_f = E_{doped-TiO_2} - E_{bulk-TiO_2} - \frac{1}{2}E_{N_2(g)}$$

Here $E_{doped-TiO_2}$ is the total energy of N-doped TiO_2-B bulk, $E_{bulk-TiO_2}$ is the total energy of TiO_2(B) bulk, $E_{N_2(g)}$ is the energy of one N_2 molecular, and $E_{O_2(g)}$ is the energy of one O_2 molecular.

The formation energy shows that the S_N4 and I_N2 sites can be formed easier than the other sites. Thus, these two sites are chosen for N doping sites in the N-doped TiO_2. Figure **7**c shows the relaxed structure of mixed N-doped TiO_2. Based on the above analysis, B doping sites in the N/B-codoped TiO_2(B) are calculated, and the

influences between defects are ignored. The codoped defects formation energy, E_f, is defined as follow and listed in Table S1.

$$E_f = E_{doped-TiO_2} - E_{bulk-TiO_2} - E_{N_2(g)} - E_{\alpha-B} + \frac{1}{2}E_{O_2(g)}$$

Here $E_{\alpha\text{-}B}$ refers to the energy of one boron atom in the TiO_2(B) bulk. The results show that site S_B4 is more stable. These structures shown in Figure 7a, c and e are employed to represent undoped TiO_2, N-doped TiO_2, N/B-codoped TiO_2 and their density of states (DOSs) are displayed in Figure 7b, d and f**.**

Supplementary Table S1. Defect formation energy of TiO_2(B).

Sites	S_N1	S_N2	S_N3	S_N4	I_N1	I_N2	I_N3	S_B1	S_B2	S_B3	S_B4
E_f/eV	5.67	5.54	5.73	5.46	4.34	4.06	5.22	13.4	12.6	12.6	12.0

We should also note that the calculated band gap of pure TiO_2(B) is about 2.344 eV (see Figure 7b) while the experimental value is reported to be 3–3.2 eV. The underestimation always exists in the band gap calculations due to the well-known limitation of the DFT theory. However, our discussions about energy gap will not be affected because only the relative energy changes are to be concerned, and the trend of the energy gap is expected to be reasonable and reliable.[1,2]

Supplementary Table S2. The diffusion coefficients (D_{Li}) of the three electrodes and the corresponding data.

Electrode	δ	dE/dx	A (cm^{-2})	D_{Li}
nanobelts	66.86	1.69	0.35	1.27 x 10^{-14}
nanotubes	5.85	0.94	1.23	5.68 x 10^{-14}
nanorods	97.92	0.85	0.46	8.72 x 10^{-15}

Supplementary references

1 Yang, K.; Dai, Y.; Huang, B.; Han, S. *J. Phys. Chem. B* **2006**, 110, 24011.

2 Yang, K.; Dai, Y.; Huang, B. *J. Phys. Chem. C* **2007**, 111, 12086.